Cancer Letters 531 (2022) 57–70

Contents lists available at ScienceDirect

Cancer Letters

journal homepage: www.elsevier.com/locate/canlet

Original Articles

Chemically synthesized cinobufagin suppresses nasopharyngeal carcinoma metastasis by inducing ENKUR to stabilize p53 expression

Rentao Hou [a,1], Xiong Liu [a,b,1,***], Huiling Yang [c,1], Shuting Deng [a,1], Chao Cheng [d,1], Jiahao Liu [a], Yonghao Li [a], Yewei Zhang [e], Jingwen Jiang [a,f], Zhibo Zhu [a], Yun Su [g], Liyang Wu [g], Yingying Xie [a], Xiaoning Li [a], Wenmin Li [a], Zhen Liu [a,h,i,**], Weiyi Fang [a,*]

[a] Cancer Center, Integrated Hospital of Traditional Chinese Medicine, Southern Medical University, Guangzhou, China
[b] Department of Otolaryngology-Head and Neck Surgery, Nanfang Hospital, Southern Medical University, Guangzhou, China
[c] School of Pharmacy, Guangdong Medical University, Dongguan, China
[d] Otolaryngology Department, Shenzhen Hospital, Southern Medical University, Guangzhou, China
[e] Hepatobiliary Surgery, Guizhou Medical University, Guiyang, Guizhou, China
[f] Oncology Department, Traditional Chinese Medicine Hospital of Hainan Provincial, Haikou, China
[g] Key Laboratory of Protein Modification and Degradation, School of Basic Medical Sciences, Affiliated Cancer Hospital and Institute of Guangzhou Medical University, Guangzhou, China
[h] Affiliated Cancer Hospital & Institute of Guangzhou Medical University, China
[i] Laboratory of Protein Modification and Degradation, State Key Laboratory of Respiratory Disease, Guangzhou Medical University, Guangzhou, China

ARTICLE INFO

Keywords:
Cancer cell metastasis
Cinobufagin
ENKUR
P53
Nasopharyngeal carcinoma

ABSTRACT

Clinically, the metastasis of tumor cells is the key factor of death in patients with cancer. In this study, we used a model of metastatic nasopharyngeal carcinoma (NPC) to explore the effects of a new chemical, cinobufagin (CB), combined with cisplatin (DDP). We observed that chemically synthesized CB strongly decreased the metastasis of NPC. Furthermore, a better therapeutic effect was shown when CB was combined with DDP. Molecular analysis revealed that CB induced ENKUR expression by deregulating the PI3K/AKT pathway and suppressing c-Jun, an oncogenic transcriptional factor that binds to the ENKUR promoter and negatively modulated its expression in NPC. ENKUR as a tumor suppressor binds to MYH9 and decreases its expression by recruiting β-catenin via its enkurin domain to prevent its nuclear accumulation, which therefore suppresses c-Jun-induced MYH9 expression. Subsequently, downregulated MYH9 reduces the enlistment of E3 ligase UBE3A and thus decreases the UBE3A-mediated ubiquitination degradation of p53, a key tumor suppressor that decreases epithelial-mesenchymal transition (EMT). Clinical sample analysis demonstrated that the ENKUR expression level was significantly reduced in NPC tissues. Its decreased expression substantially promoted clinical progression and reflected poor prognosis for patients with NPC. This study demonstrated that CB induced ENKUR to repress the β-catenin/c-Jun/MYH9 signal and thus decreased UBE3A-mediated p53 ubiquitination degradation. As a result, the EMT signal was inactivated to suppress NPC metastasis.

1. Introduction

Some well-confined primary tumors can be cured by surgical resection, adjuvant therapy, and other means [1–4]. However, metastatic tumors are largely incurable because of their systemic nature and tumor cell resistance to therapeutic agents. These features explain why more than 90% of mortality is attributable to metastatic tumor lesions [5]. Thus, new drug candidates that are effective against tumor metastases will improve the overall survival for patients.

cinobufagin is extracted from the skin secretions of giant toads for clinical use in traditional Chinese medicine; it has been used widely for many years to treat multiple types of carcinomas [6–8]. CB plays a

* Corresponding author. Cancer Center, Integrated Hospital of Traditional Chinese Medicine, Southern Medical University, Guangzhou, Guangdong, China.
** Corresponding author. Affiliated Cancer Hospital & Institute of Guangzhou Medical University, China.
*** Corresponding author.
E-mail addresses: liux1218@126.com (X. Liu), narcissus_jane@163.com (Z. Liu), fangweiyi1975@163.com (W. Fang).
[1] These authors contributed equally: Rentao Hou, Xiong Liu, Huiling Yang, Shuting Deng, Chao Cheng.

https://doi.org/10.1016/j.canlet.2022.01.025
Received 23 May 2021; Received in revised form 1 January 2022; Accepted 19 January 2022
Available online 1 February 2022

crucial role in several cancers by inhibiting cancer cell proliferation and apoptosis [9–12]. Recently, we explored the role of CB as a small-molecule drug formulation in nasopharyngeal carcinoma (NPC) and found that CB inhibited tumor stemness and cisplatin (DDP) resistance by modulating EBV-miR-BART22/MAP2K4-mediated MYH9/GSK3β/β-catenin signals and FOXO1/MYH9-mediated epithelial-mesenchymal transition (EMT) signals [13,14]. However, the anti-metastatic effect of CB on tumors and the molecular mechanisms driving CB activity remain undetermined.

In this study, we used a model of NPC to probe the therapeutic effect of CB combined with DDP for cancer metastasis, and we demonstrated that chemically synthesized CB powerfully decreased the metastasis of NPC by inducing the expression of ENKUR via PI3K/AKT/c-Jun axis. We also found that ENKUR or its enkurin domain bound to MYH9 and repressed the β-catenin/c-Jun/MYH9 signal-mediated ubiquitination of p53 by decreasing the enlisting E3 ligase UBE3A to decrease EMT signals. Our study revealed that CB is an important anti-tumor drug for tumor metastasis that acts by inducing ENKUR to increase MYH9-mediated deubiquitination of p53. As such, CB may become a novel treatment for patients with metastases.

2. Materials and methods

2.1. Cell culture

5–8F cells and HONE-1 cells were stored at the Cancer Research Institute of the Southern Medical University (Guangzhou, China). All cell lines were cultured in RPMI-1640 (Huixiang Biotechnology Co., Ltd., Guangzhou, China) supplemented with 10% fetal bovine serum (Haoyue Biotechnology Co., Ltd., Guangzhou, China) and were maintained in a humidified, 5% CO_2 incubator at 37 °C.

2.2. Lentivirus production and infection

Lentiviral particles carrying the ENKUR precursor and control vectors were constructed by GeneChem (Shanghai, China). 5–8F and HONE-1 cells were infected with lentiviral or control vectors, respectively. Green fluorescent protein was used as the marker to monitor infection efficiency. Overexpressing efficiency of ENKUR was validated by western blot.

2.3. Transient transfection

Si-RNAs for ENKUR were designed and synthesized at RiboBio, Inc. (Guangzhou, China)(Supporting Information Table S1). C-Jun, β-catenin, and MYH9 plasmids were purchased from Vigene Biosciences (Shandong, China). ENKUR and ENKUR domain plasmids were purchased from GeneChem (Shanghai, China). MYH9 domain plasmids were purchased from BersinBio (Guangzhou, China). NPC cells were plated onto a six-well plate (Nest Biotech, China) at 30%–50% confluence. The si-RNAs or plasmids were transfected into cells using Lipofectamine TM 2000 (Invitrogen Biotechnology, China) according to the manufacturer's protocol. After 48–72 h, cells were collected for additional experiments.

2.4. RNA isolation, RT-PCR, qPCR, and primers

Total RNA was collected from NPC cells using a TRIzol reagent (Takara, Shiga, Japan). RNA was reverse transcribed into complementary DNA according to the manufacturer's instructions (TaKaRa, Dalian, China). Qualitative reverse transcriptase PCR was performed in triplicate with SYBR Premix ExTaq (TaKaRa, Dalian, China). Specific primers are shown in Supplementary Table S2.

2.5. Western blot analysis, reagents, and antibodies

Cell lysates were separated by SDS-PAGE followed by blocking in 3% BSA (Bovine Serum Albumin) and then incubated with primary antibodies against anti-ENKUR, PI3K, p-PI3K, AKT, p-AKT, β-catenin, c-Jun, MYH9, p53, UBE3A, ubiquitin, E-cadherin, N-cadherin, Snail, β-actin, and GADPH. Information about these antibodies is presented in Supplementary Table S3. The immunoreactive bands were visualized with chemiluminescence (Millipore, Bedford, MA, USA), and images were captured with the Minichemi Imaging System (Sage, Beijing, China). All blot figures include the location of molecular weight/size markers.

2.6. MTT assay

The drug sensitivity was tested by MTT assays. CB was dissolved in dimethyl sulfoxide (DMSO; Sigma, St. Louis, MO, USA) and adjusted to 50 mM before further dilution with media. Then, 5×10^3 cells/well were plated into 96-well plates and treated with 0, 200, 400, 600, 800, and 1000 nmol of CB or DDP for 48 h. Subsequently, 20 μL of MTT (5 mg/mL; Sigma, St. Louis, MO, USA) was added to each well and cultivated at 37 °C for 4 h. Finally, the reagent in the wells was replaced with 150 μL of DMSO, and the optical density of each well was measured at 490 nm.

2.7. Wound healing assay

5–8F and HONE-1 cells were inoculated in six-well plates and transfected with plasmids or si-RNAs overnight. Then, cells were wounded by dragging a 1000 μL pipette tip across the center of the well and were treated with serum-free RPMI 1640 medium. The cell migration ability was assessed by measuring the distance traveled into the wound at 0 and 48 h after scratching.

2.8. Boyden assay

Boyden assays (Millipore, Bedford, MA, USA) were performed to determine the invasion ability of NPC cells using cell culture inserts (Corning, New York, USA). After transwell membranes were coated with 24 μg/mL of Matrigel (R&D Systems, USA) for 30 min, approximately 8×10^4 cells were stored in 100 μL of RPMI-1640 without serum and seeded into the top chamber of the transwells; the bottom chambers were filled with 500 μL of RPMI-1640 supplemented with 10% fetal bovine serum. After 13 h, the non-migrated cells were removed and the filter was fixed, stained, and photographed. Cells were counted under a microscope in three random fields.

2.9. ChIP

Two putative c-Jun-binding sites on the ENKUR promoter region were predicted through the JASPAR and ALGGEN databases. The ENKUR and c-Jun complexes from 5 to 8F and HONE-1 cells were tested according to the manufacturer's protocol (Thermo Fisher Scientific), and chromatin was crosslinked, isolated, and digested with Micrococcal Nuclease to obtain DNA fragments. The anti-c-Jun antibody (1:50, Cell Signaling Technology, USA) or IgG was added to the reaction systems for immunoprecipitation. Finally, the DNA fragments were tested by qualitative PCR with specific primers.

2.10. Co-IP assay

Co-IP was conducted with a Pierce coimmunoprecipitation kit (Thermo Scientific, USA) according to the manufacturer's directions. Broadly, approximately 1000 μg of protein was incubated with 10 μg of special antibodies overnight at 4 °C. Then, the immune complexes were washed, eluted, and analyzed by western blot. Anti-IgG was used as a negative control.

2.11. Immunofluorescence and confocal microscopy

NPC cells were plated onto coverslips in 48-well plates and cultured overnight to allow cell adherence. Then, cells were treated with 4% paraformaldehyde and underwent permeabilization in 0.2% Triton X-100 for approximately 30 min. Subsequently, suitable concentrations of antibodies were added to NPC cells and incubated overnight. On the second day, the coverslips were incubated with DAPI for 5 min and visualized with a fluorescent confocal microscope.

2.12. Nuclear and cytoplasmic extraction

Nuclear and cytoplasmic separations were conducted with an NE-PER nuclear and cytoplasmic extraction kit (Thermo Scientific, Waltham, MA, USA) according to the manufacturer's directions. NPC cells were incubated with ice-cold CER I for 10 min at 4 °C; then CER II was added for 1 min and the mixture was centrifuged at 16,000×*g* for 5 min. The pellet was resuspended in a NER extraction regent and incubated for 40 min on ice. After the suspension was centrifuged, protein was obtained and analyzed by western blot.

2.13. CHX chase assay

NPC cells were transfected with scrambles or plasmids and then either combined with 20 μmol/L of MG132 (Sigma-Aldrich, MO, USA) for 6 h or left untreated. The cells were treated with 50 μg/mL of CHX (Abcam, Massachusetts, USA), and the proteins were prepared for western blot.

2.14. IHC

Paraffin sections (4-μm thick) from clinical samples were stored at the Nanfang Hospital, Southern Medical University (Guangzhou, China). These sections were deparaffinized and heated in an antigen-unmasking solution for 3 min at 100 °C. Then, nonspecific antigens and endogenous peroxidase activity were blocked with 3% H_2O_2 and goat serum, and slides were incubated with antibodies overnight at 4 °C. Sections were incubated with horseradish peroxidase-conjugated secondary antibody and visualized using a DAB substrate and analyzed under a brightfield microscope. The score was evaluated according to the percentage of positive-staining areas (1: <25%, 2:25% to <50%, 3:50% to <75%, 4: ≥75%) and cytoplasmic staining intensity of the cells (0 = negative, 1 = weakly positive, 2 = moderate positive, 3 = strongly positive); the final score was calculated by multiplying the percentage score by the intensity score. A final score of 6 or lower was defined as low expression, and the remaining scores were considered high expression.

2.15. EMSA

The EMSA (BersinBio, Guangzhou, China) was used according to the manufacturer's directions. Nuclear extracts were obtained from NPC cells and mixed with biotin-labeled probes after the concentration was tested. Competition assays were performed with unlabeled wild-type or mutant probes, and supershift assays were performed with anti-c-Jun antibodies. Signals were recorded using a BioSens Gel Imaging System (BIOTOP).

2.16. In vivo metastasis assays

All mice were 4 weeks old, were female, and weighed 8–10 g; they were purchased from the Shanghai Laboratory Animal Center (Shanghai, China). Approximately 100 μL of 5–8F overexpressing ENKUR or control cells (4×10^6) were injected into the tail vein of each mouse (five mice per group). All mice were killed after 6 weeks and their lung tissues were removed; the metastatic tissues were analyzed under fluorescence microscopy. All animals were treated according to the principles and procedures outlined in the Southern Medical University Guide for the Care and Use of Animals.

2.17. Treatment experiments on nude mice

All mice were divided into four groups (normal saline, CB, DDP, and CB + DDP) after NPC cells were injected for 8 days. Mice were injected intraperitoneally with saline, CB (4 mg/kg), DDP (4 mg/kg) or CB (4 mg/kg) + DDP (4 mg/kg) once every 3 days. All in vivo experiments were approved by the Animal Care and Use Committee of Southern Medical University.

2.18. Statistical analysis

All statistical analyses were performed using SPSS version 24.0 (SPSS, Inc., Chicago, IL, USA). Data were expressed as the means ± standard deviations. Student's t-test was used to analyze two groups. Analysis of variance was used to analyze more than two groups. The relationship between ENKUR expression and clinicopathological factors was determined by chi-square testing. The survival analysis was performed using the Kaplan-Meier method. All statistical tests were two sided, and a P value of <0.05 was considered statistically significant. *P < 0.05, **P < 0.01 and ***P < 0.001.

3. Results

3.1. CB inhibited tumor migration, invasion, and metastasis in NPC

The half maximal inhibitory concentrations (IC50s) of CB in 5–8F and HONE-1 cells were 446.0 nM and 627.6 nM, respectively; these results were much lower than concentrations for DDP (Fig. 1A). We used concentrations of 500 nM and 750 nM, respectively, to treat the 5–8F and HONE-1 NPC cells in the following experiments. After CB treatment, the cells showed worse migration and poorer invasion ability compared with the control group cells on a wound healing assay (Fig. 1B, S1A) and a Boyden assay (Fig. 1C, S1B). Moreover, we detected the key signals of EMT by western blot and found that N-cadherin and Snail were down-regulated, whereas E-cadherin was increased, after treatment with CB (Fig. 1D). These data indicated that CB suppressed tumor migration and invasion.

Finally, we performed an in vivo experiment to investigate the effect of CB in tumor metastasis. We generated a model of lung metastasis with lentivirus-infected 5–8F cells and assessed four different treatment groups: normal saline, DDP(4 mg/kg), CB(4 mg/kg), and CB(4 mg/kg) + DDP(4 mg/kg). Lung tissues were removed from the mice after 5 weeks of injections. All three groups treated with drugs showed fewer metastatic lung tumors and lower expressions of green fluorescent lentiviral markers compared with the normal saline group. No significant differences existed between the CB and DDP groups in anti-metastatic ability, but the CB + DDP group displayed the lowest expression of green fluorescent lentiviral markers (Fig. 1E, S1C). In addition, immunohistochemistry (IHC) assays indicated that CB and CB + DDP groups had higher E-cadherin and lower N-cadherin levels compared with the saline group (Fig. 1F). These data showed that CB decreased the ability of NPC to migrate, invade, and metastasize.

3.2. ENKUR induced by CB functions as an anti-tumor metastasis factor

The expression level of ENKUR was significantly reduced in NPC cells compared with NP cells (Fig. S2A). A previous study showed that marinobufagenin, whose chemical structure is similar to CB(Fig. S2B) could induce ENKUR in brain endothelial cells. So CB was added to NPC cells, qualitative polymerase chain reaction (PCR) analysis revealed a significantly upregulated mRNA level of ENKUR (Fig. 2A). To explore the effect of ENKUR on tumor metastasis, the lentiviral vectors carrying ENKUR or control vectors were infected into 5–8F and HONE-1 cell lines

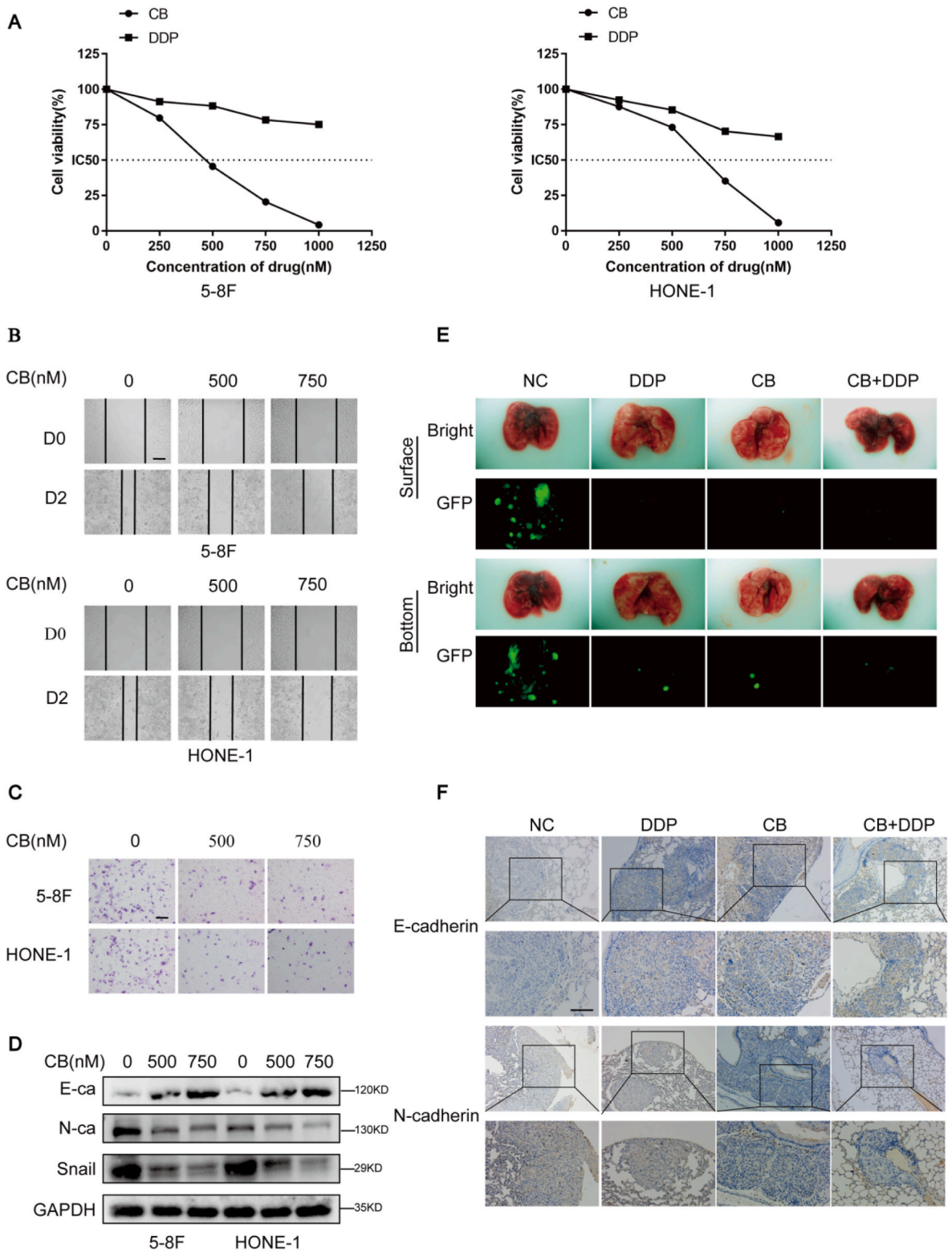

Fig. 1. Cinobufagin (CB) inhibited tumor migration, invasion, and metastasis in nasopharyngeal carcinoma (NPC). (A) Dose-response curves are shown in 5–8F and HONE-1 cells treated with CB or cisplatin (DDP) for 48 h. (B) Wound healing assays (scale bar:200 μm) and (C) Boyden assays (scale bar:200 μm) were performed in CB-treated NPC cells and control cells. (D) Western blot analysis of E-cadherin, N-cadherin, and Snail in CB-treated 5–8F and HONE-1 cells. (E) Pulmonary metastasis models were used to compare the effect of CB (4 mg/kg), DDP (4 mg/kg), or CB(4 mg/kg) combined with DDP(4 mg/kg) on metastasis. (F) Immunohistochemistry was used to show the expression of E-cadherin and N-cadherin in models of lung metastasis. (scale bar:250 μm).

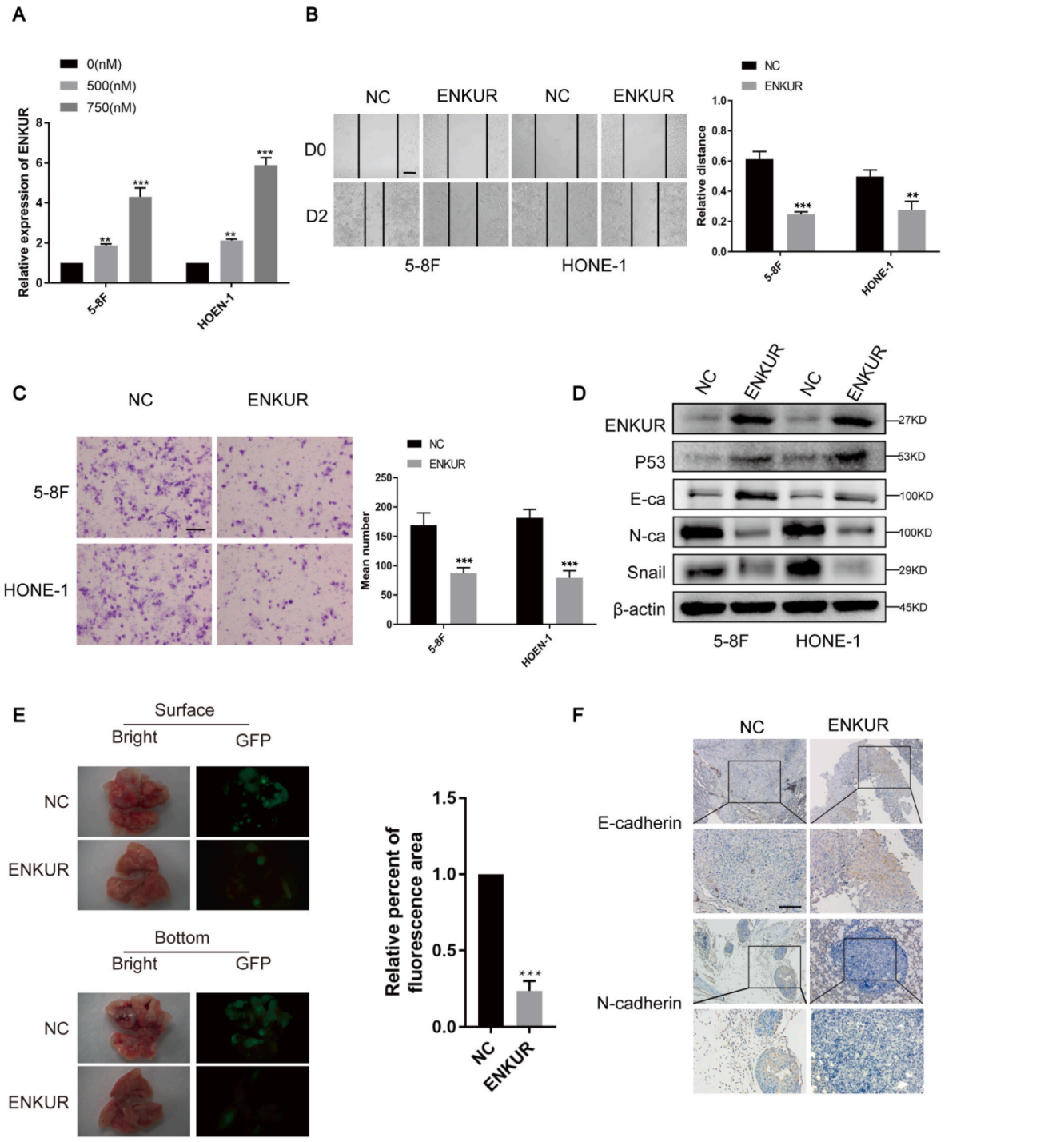

Fig. 2. ENKUR induced by cinobufagin (CB) functions as a factor in anti-tumor metastasis. (A) QPCR analysis of ENKUR in 5–8F and HONE-1 cells treated with CB. (B)Wound healing assays (scale bar:200 μm) and (C) Boyden assays (scale bar:200 μm) were performed in ENKUR-overexpressing nasopharyngeal carcinoma (NPC) cells and control cells. (D) The protein levels of ENKUR, p53, E-cadherin, N-cadherin, and Snail were measured in ENKUR-overexpressing 5–8F and HONE-1 cells. (E) Modes of pulmonary metastasis were established to investigate the effect of ENKUR on metastasis. (F) Immunohistochemistry was used to detect the expression of E-cadherin and N-cadherin in lung metastasis models. (scale bar:250 μm).

(Fig. S2C). The overexpressing ENKUR in NPC cells had lower migration and invasion capacities on a wound healing assay (Fig. 2B) and a Boyden assay (Fig. 2C). Western blot was used to detect p53 and the key factors of EMT. Results showed that p53 was increased and the EMT pathway was silenced in cells overexpressing ENKUR; including E-cadherin was upregulated, and N-cadherin and Snail were downregulated (Fig. 2D). The models of pulmonary metastasis were established by tail-vein injection with a control vector or an ENKUR-overexpressing vector in 5–8F cells. Compared with the control group, the ENKUR-overexpressing group showed fewer lung tumor metastases (Fig. 2E), higher E-cadherin expression, and lower N-cadherin expression (Fig. 2F). Furthermore, silencing ENKUR expression through its specific si-RNA (Fig. S2D) stimulated the invasion and migration capabilities on the Boyden assay (Fig. S2E) and the wound healing assay (Fig. S2F) in 5–8F and HONE-1 cells overexpressing ENKUR. Western blot indicated that the inducing effect of ENKUR on p53 and the inhibitory effect on EMT-related

proteins were reversed after knocking down ENKUR (Fig. S2G). Together, these data demonstrate the anti-metastatic ability of ENKUR in NPC.

3.3. ENKUR binds to MYH9

We have demonstrated that MYH9 is a potential interaction protein of ENKUR by mass spectrometry analysis and a coimmunoprecipitation (co-IP) assay in A549 cells (data not published). An immunofluorescence assay showed that ENKUR colocalized in the cytoplasm with MYH9 in 5–8F and HONE-1 cells (Fig. 3A). Co-IP examinations of 5–8F and HONE-1 cells confirmed that MYH9 combined to ENKUR (Fig. 3B). ENKUR contains three domains: the N-terminal region domain, the SH3 domain, and the enkurin domain (Fig. 3C); on wound healing and Boyden assays, only the enkurin domain demonstrated anti-migration and anti-invasion abilities in NPC cells (Fig. S3A-B). Furthermore, the enkurin domain, but not the other two domains, combined with MYH9 (Fig. 3D). MYH9 also contains three domains: myosin_N, myosin_head_motor, and myosin_tail (Fig. 3E). Functional experiments indicated that the myosin_tail domain was the key factor to promotion of cell migration and invasion in NPC cells (Fig. S3C-D). On the co-IP assay, only the myosin_tail interacted with ENKUR (Fig. 3F). MYH9 plasmids were transfected into ENKUR-overexpressing NPC cells and the migration and invasion inhibition of ENKUR was reversed via wound healing and boyden assays in NPC (Fig. S3E-F).

3.4. ENKUR interacts with β-catenin and decreases MYH9 expression

An immunofluorescence assay revealed that ENKUR and β-catenin colocalize in the cytoplasm (Fig. 4A), and co-IP showed that ENKUR interacts with β-catenin in 5–8F and HONE-1 cells overexpressing ENKUR (Fig. 4B). Furthermore, the Enkurin domain bound to β-catenin (Fig. 4C). Although overexpressing ENKUR did not change the total protein expression of β-catenin (Fig. 4D), it reduced the nuclear accumulation of β-catenin protein and increased the cytoplasmic protein level of β-catenin (Fig. 4E). ENKUR overexpression downregulated the mRNA level of MYH9 in NPC cells (Fig. 4F), and western blot showed that c-Jun and MYH9 protein levels were decreased in NPC (Fig. 4D). In previous study, we confirmed that β-catenin/c-Jun-dependent transcription upregulated MYH9 in HCC [15]. In this study, overexpressing β-catenin promoted the nuclear translocation of β-catenin and reversed the ENKUR inhibition of c-Jun and MYH9 in overexpressing ENKUR NPC cells (Fig. S4A-B). Thus, we conclude that ENKUR downregulated MYH9 via the β-catenin/c-Jun axis.

3.5. MYH9 recruits UBE3A to facilitate degradation of p53 ubiquitination

We showed that ENKUR increased the protein level of p53 (Fig. 2D). In this study, western blot indicated that MYH9 restored the p53 expression and inhibition of EMT signals in ENKUR-overexpressing NPC cells (Fig. 5A). However, MYH9 overexpression did not change the mRNA level of p53 (Fig. 5B). Thus, ENKUR might inhibit EMT via MYH9-mediated degradation of p53 ubiquitination. To clarify this hypothesis, 40 μM of cycloheximide (CHX) was introduced into ENKUR-overexpressing NPC cells and control cells; results showed that p53 had a longer half life in ENKUR-overexpressing cells than in the control cells. In addition, overexpressing MYH9 reversed the alterations in the p53 half life. The half-life of p53 remained unchanged when cells were treated with a reversible proteasome inhibitor, MG132 (Fig. 5C). Research has shown that UBE3A, an E3 ubiquitin ligase, interacts with p53 and decreases its expression [16–18]. The GeneMANIA database was used to predict the interaction of the MYH9 protein with UBE3A and p53 (Fig. S4C). The co-IP assay demonstrated that MYH9 recruits UBE3A to degrade of p53 by ubiquitination (Fig. 5D). Injection of a plasmid carrying MYH9 into ENKUR-overexpressing 5–8F cells showed that MYH9 overexpression increased the interaction between p53 and UBE3A (Fig. 5E).

3.6. CB promotes ENKUR through the PI3K/AKT/c-Jun axis

We have shown that CB induces ENKUR expression. The results of the Boyden assay and the wound healing assay revealed that silencing ENKUR restored the invasion and migration ability of NPC cells treated with CB (Fig. S5A-B).Western blot showed that c-Jun, MYH9, N-cadherin and Snail were increased, whereas E-cadherin, p53 and ENKUR were decreased after CB treatment with si-RNA for ENKUR in NPC cells (Fig. S5C). To explore how CB mediated ENKUR in NPC, two c-Jun binding sites were predicted by the JASPAR and ALGGEN databases (Fig. 6A). c-Jun was able to decrease ENKUR expression when it was overexpressed in 5–8F and HONE-1 cells in mRNA and at the protein level (Fig. 6B and C). Qualitative PCR and gel electrophoresis after chromagen immunoprecipitation (ChIP) verified that c-Jun bound to the promoter region of ENKUR (Fig. 6D and E). Electrophoretic mobility shift assays (EMSAs) then demonstrated that c-Jun bound to the ENKUR promoter (Fig. 6F). The luciferase reporter assays confirmed markedly upregulated luciferase activity in NPC cells after c-Jun cDNA transfection compared with that of the control cells (Fig. 6G). Furthermore, western blot showed that CB combined with PI3K inhibitor LY294002 synergistically downregulated p-PI3K, p-AKT, and c-Jun and upregulated ENKUR in NPC cell (Fig. 6H). According to these data, CB induces ENKUR by activating PI3K/AKT/c-Jun-mediated transcription repression.

3.7. Clinicopathologic characteristics of ENKUR expression in NPC

We confirmed that ENKUR expression was upregulated in NP tissue compared with NPC tissue (Fig. 7A, Table 1). The clinical characteristics of the patients with NPC are summarized in Table 2. There was no significant association between ENKUR expression and age, sex, or N stage of patients, but clinical stage ($P = 0.038$), T stage ($P = 0.026$), and M stage ($P = 0.020$) were significantly associated with ENKUR expression. In addition, those who had high levels of ENKUR expression had longer survival times compared with patients who had low levels of ENKUR expression of ENKUR (log-rank test, $P = 0.007$, Fig. 7B). A subsequent stratum analysis showed that high ENKUR expression positively correlated with the survival time of advanced-stage, but not early-stage, disease (Fig. 7C and D). Univariate and multivariate Cox regression analyses in 121 patients with NPC showed that ENKUR expression, clinical stage and M classification were independent prognostic factors (Table 3).

4. Discussion

Metastasis is one of the most common causes of death in patients with cancer [19,20]. NPC has the highest metastasis rate among head and neck cancers [21], and distant metastasis of NPC may cause treatment failure [22]. DDP and 5-fluorouracil as the first-line therapies to treat NPC mainly promote cell apoptosis and block the cell cycle [23–26]. Their long-term use will produce drug resistance and increase the risk of EMT and metastasis [27–29]. Thus, a novel medicine to treat metastases of NPC is urgently needed.

Traditionally sourced CB is a bufadienolide extracted from toad venom, and it has anticancer activity [30,31]. Our previous studies have shown that a small-molecule drug formulation of CB inhibits DDP resistance and stemness in NPC cells [13,14]. However, to our knowledge, no in vivo experiments have been conducted to explore the potential for CB to block NPC metastasis. In this study, we found that CB treatment suppresses NPC cell invasion and migration and inactivated EMT signal in vitro. Then, in vivo experiments were conducted to verify the suppressive effect of CB on NPC metastasis and anti-metastasis ability of CB is similar to that of DDP. In addition, CB combined with

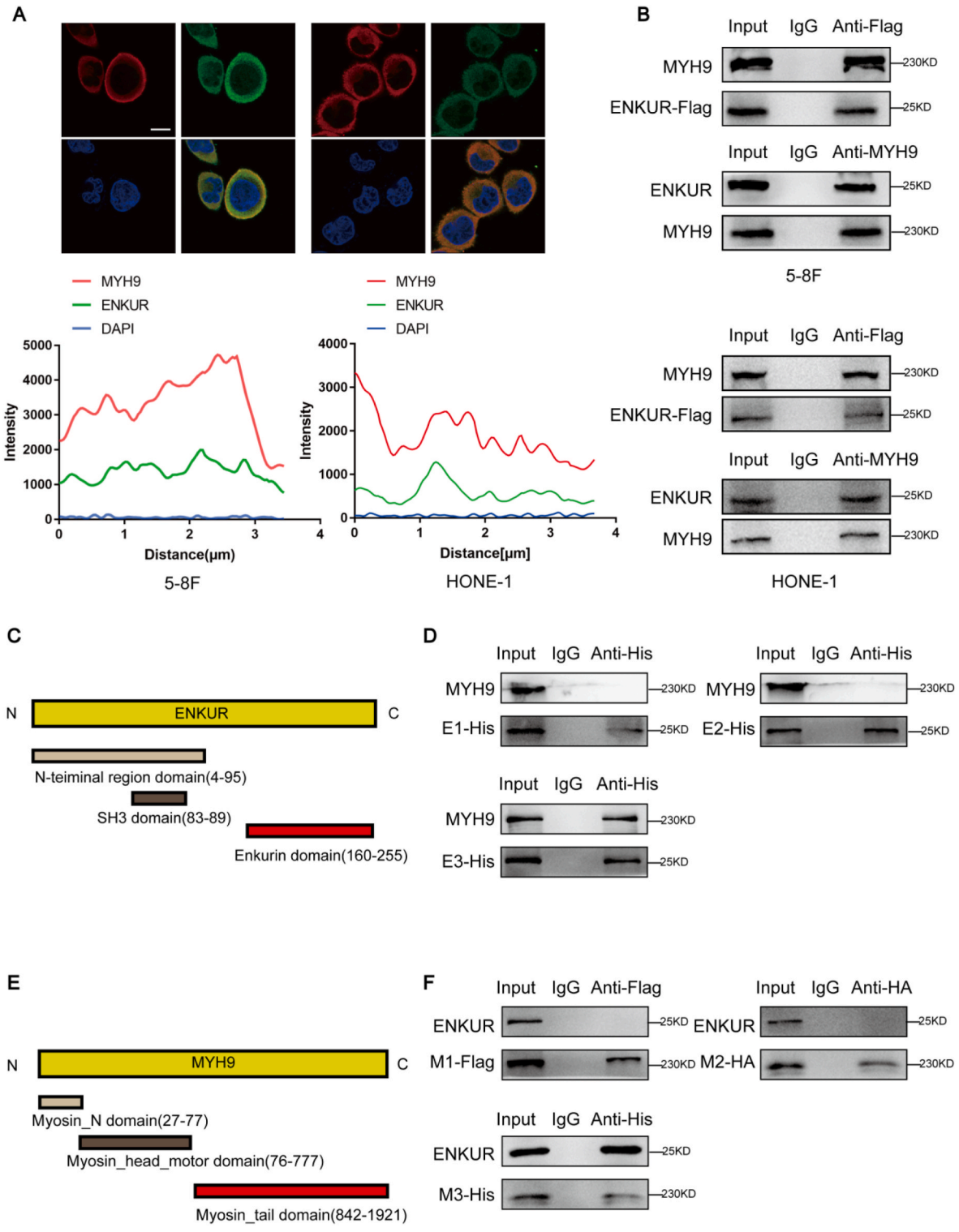

Fig. 3. ENKUR binds to MYH9. (A) Immunofluorescence costaining of MYH9 and ENKUR to detect colocalization. The red or green curves mean MYH9 or ENKUR respectively, and the same upward and downward trend of curves means they are co-located in the same location.(B) Coimmunoprecipitation analysis was performed to assess the interaction between ENKUR and MYH9 in ENKUR-overexpressing 5–8F and HONE-1 cells. (C) A schematic diagram of the domains in ENKUR is shown. (D) Coimmunoprecipitation analysis was used to determine the interaction between domains of ENKUR and MYH9 in 5–8F cells transfected with plasmids containing different ENKUR domains. (E) A schematic diagram of the domains in MYH9 is shown. (F) Coimmunoprecipitation analysis was used to determine the interaction between domains of MYH9 and ENKUR in 5–8F cells transfected with plasmids containing different MYH9 domains. (For interpretation of the references to color in this figure legend, the reader is referred to the Web version of this article.)

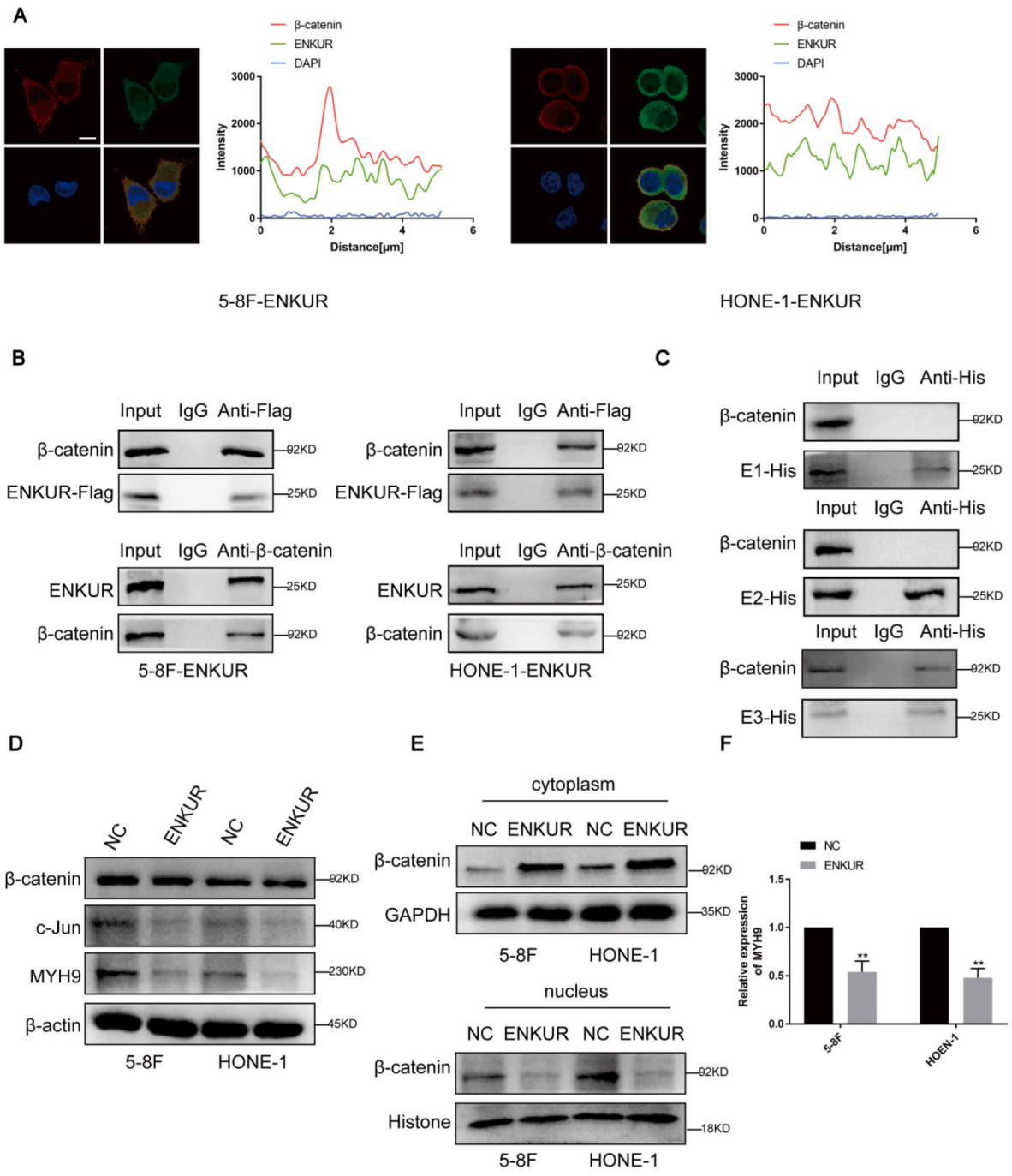

Fig. 4. ENKUR interacts with β-catenin and decreases MYH9 expression. (A) Immunofluorescence staining was applied to show the interaction between ENKUR and β-catenin in ENKUR-overexpressing 5–8F and HONE-1 cells.The red or green curves mean β-catenin or ENKUR respectively, and the same upward and downward trend of curves means they are co-located in the same location. (scale bar:25 μm) (B) Coimmunoprecipitation analysis was used to determine the interaction between ENKUR and β-catenin in ENKUR-overexpressing 5–8F and HONE-1 cells. (C) Coimmunoprecipitation analysis was used to determine the interaction between domains of ENKUR and β-catenin in 5–8F cells transfected with plasmids containing different ENKUR domains. (D) The protein levels of β-catenin, c-Jun, and MYH9 in NPC cells transfected with ENKUR plasmids and control cells are shown. (E) The expression of β-catenin in the cytoplasm and nucleus of NPC cells was determined with or without ENKUR overexpression. (F) QPCR analysis of MYH9 in 5–8F and HONE-1 cells with or without ENKUR overexpression. (For interpretation of the references to color in this figure legend, the reader is referred to the Web version of this article.)

DDP showed the most powerful anti-metastasis ability of NPC. IHC analysis detected the EMT signal protein, and groups treated with drugs had higher E-cadherin and lower N-cadherin levels compared with the untreated (normal saline) group. These data demonstrated that CB inhibits the metastasis of NPC by inactivating EMT signals but did not clarify the mechanism of action.

ENKUR reportedly is an adaptor that localizes calcium-sensitive signal transduction machinery in sperm to a calcium-permeable ion channel [32]. Research shows that ENKUR is an anti-tumor gene in colorectal cancer and lung adenocarcinoma [33,34]. Interestingly, in human brain microvascular endothelial cells, ENKUR mRNA concentrations were upregulated after treatment with marinobufagenin, a bufotoxin [35]. We hypothesized that chemically synthesized CB would regulate ENKUR expression in NPC cells. Qualitative PCR was conducted

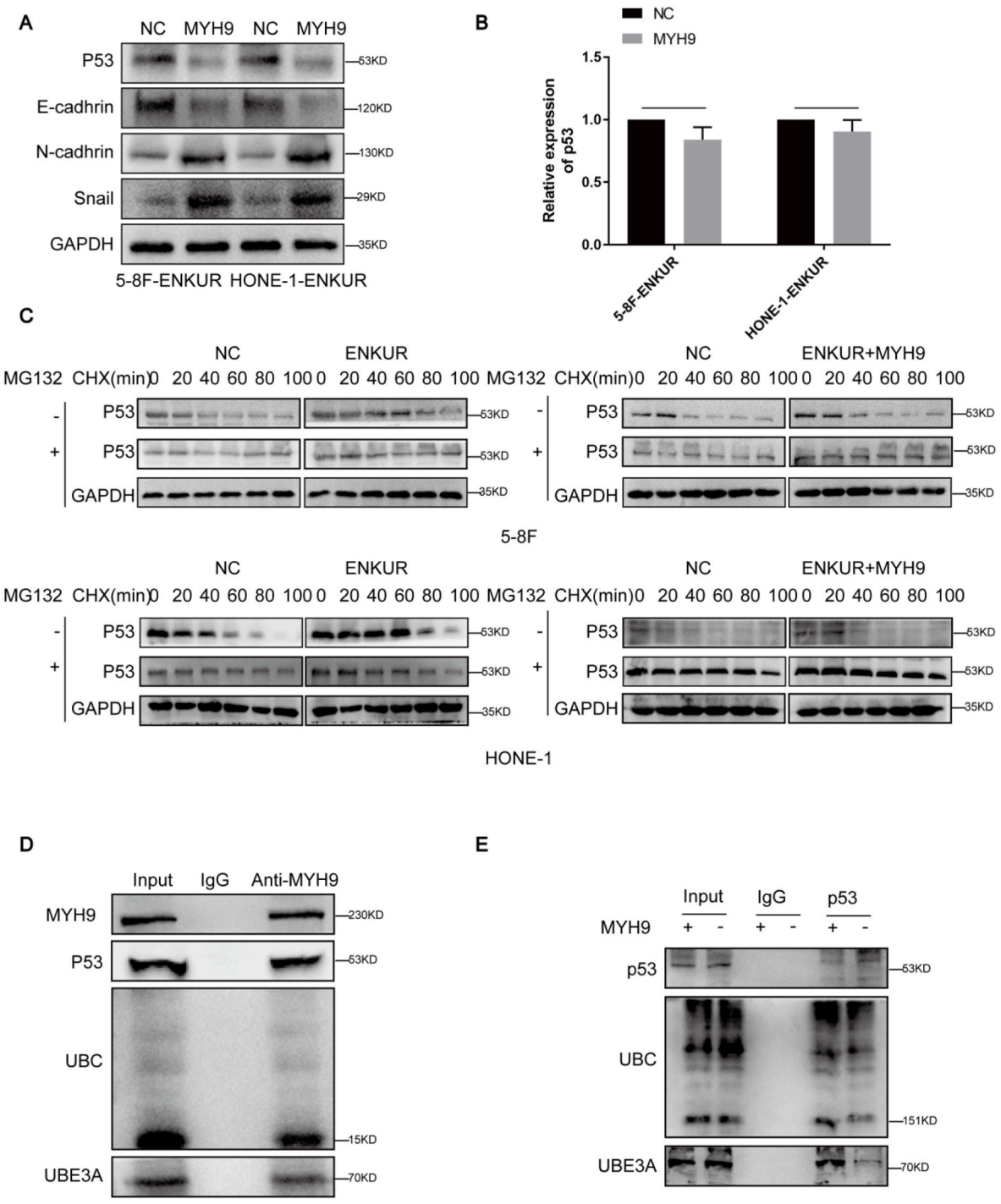

Fig. 5. MYH9 recruits UBE3A to facilitate degradation of p53 ubiquitination. (A) The effect of MYH9 transfection on the protein levels of p53, E-cadherin, N-cadherin, and Snail were measured in ENKUR-overexpressing 5–8F and HONE-1 cells. (B) QPCR analysis of p53 in ENKUR-overexpressing 5–8F and HONE-1 with an MYHP plasmid. (C) Western blotting and quantification analyses were used to analyze the effect of ENKUR and MYH9 on p53 stability in nasopharyngeal carcinoma (NPC) cells incubated with cycloheximide at different time points with or without MG132. (D) The interactions of MYH9, UBE3A, p53, and ubiquitin were detected in 5–8F cells. (E) Coimmunoprecipitation analysis of the effect of MYH9 on the interaction between p53, ubiquitin, and UBE3A in 5–8F cells.

in CB-treated NPC cells and showed that ENKUR expression increased with increasing concentrations of CB. Furthermore, we confirmed that ENKUR functioned as an anti-metastasis factor in NPC by studying the invasion and migration effects in vitro and the pulmonary metastasis mode in vivo. Preliminarily mechanistic analysis indicated that ENKUR suppressed the EMT signal pathway. Knocking down ENKUR expression recovered the migration and invasion in ENKUR-overexpressing NPC cells. These data suggested that ENKUR inhibits tumor metastasis by participating in CB-mediated metastasis suppression of NPC.

In previous studies, we demonstrated that MYH9 acts as a tumor promoter by interacting with HBX, FOXO1, or GSK3β in hepatocellular carcinoma (HCC) and NPC [13–15]. In this study, we found that MYH9 is also a potential binding protein of ENKUR, as demonstrated by co-IP coupling with mass spectrometry in ENKUR-overexpressing A549 cells (data not published). We confirmed that ENKUR combined with MYH9 and colocalized in the cytoplasm. Domains are distinct units within

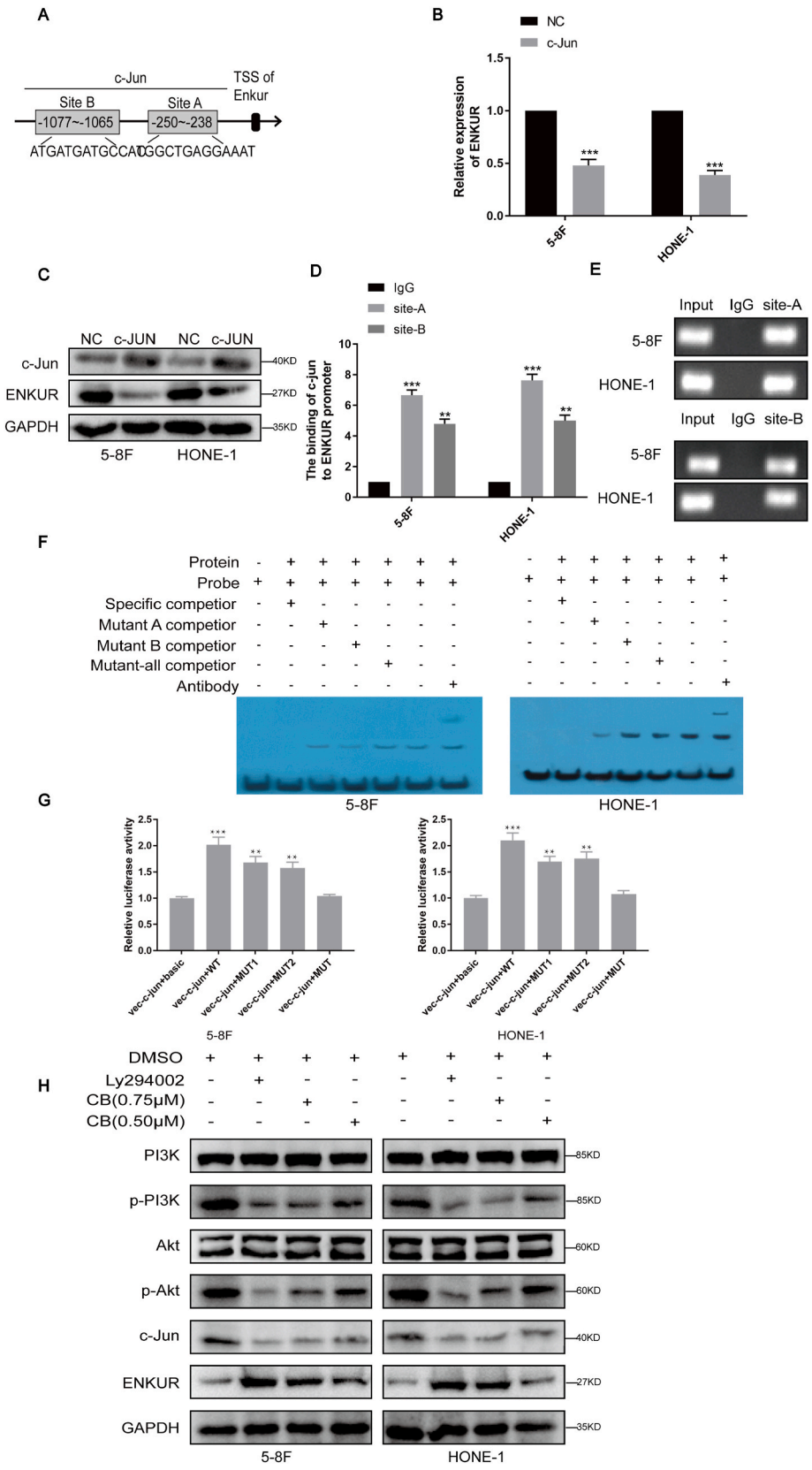

Fig. 6. cinobufagin (CB) promoted ENKUR through the PI3K/AKT/c-Jun axis. (A) Bioinformatics analysis was used to predict the binding sites of c-Jun within the promoter of ENKUR. (B) QPCR analysis of c-Jun in 5–8F and HONE-1 cells with or without ENKUR overexpression. (C) The protein levels of c-Jun and ENKUR were measured in c-Jun-overexpressing 5–8F and HONE-1 cells. (D) Chromatin immunoprecipitation (ChIP) assays were used to detect the binding of c-Jun to the ENKUR promoter in nasopharyngeal carcinoma (NPC) cells. (E) Gel electrophoresis after ChIP. (F) The protein-DNA interactions between c-Jun and the ENKUR promoter were determined using the electrophoretic mobility shift assay. **(G)** Luciferase reporter assays were performed to confirm c-Jun binding to the ENKUR promoter. (H)The protein levels of PI3K, p-PI3K, AKT, p-AKT, c-Jun, and ENKUR were detected in 5–8F and HONE-1 cells treated with CB or LY294002.

proteins and provide the key functional building blocks of proteins [36, 37]. ENKUR was predicted to contain three domains: the N-terminal region domain, SH3 domain, and enkurin domain. MYH9 was predicted to have three domains: myosin_N, myosin_head_motor, and myosin_tail. After different plasmids were injected with different domains of ENKUR and MYH9, tests showed that the enkurin domain exerted a tumor suppressor function and the myosin_tail domain functioned as an oncogene in 5–8F and HONE-1 cells. In addition, enkurin bound to

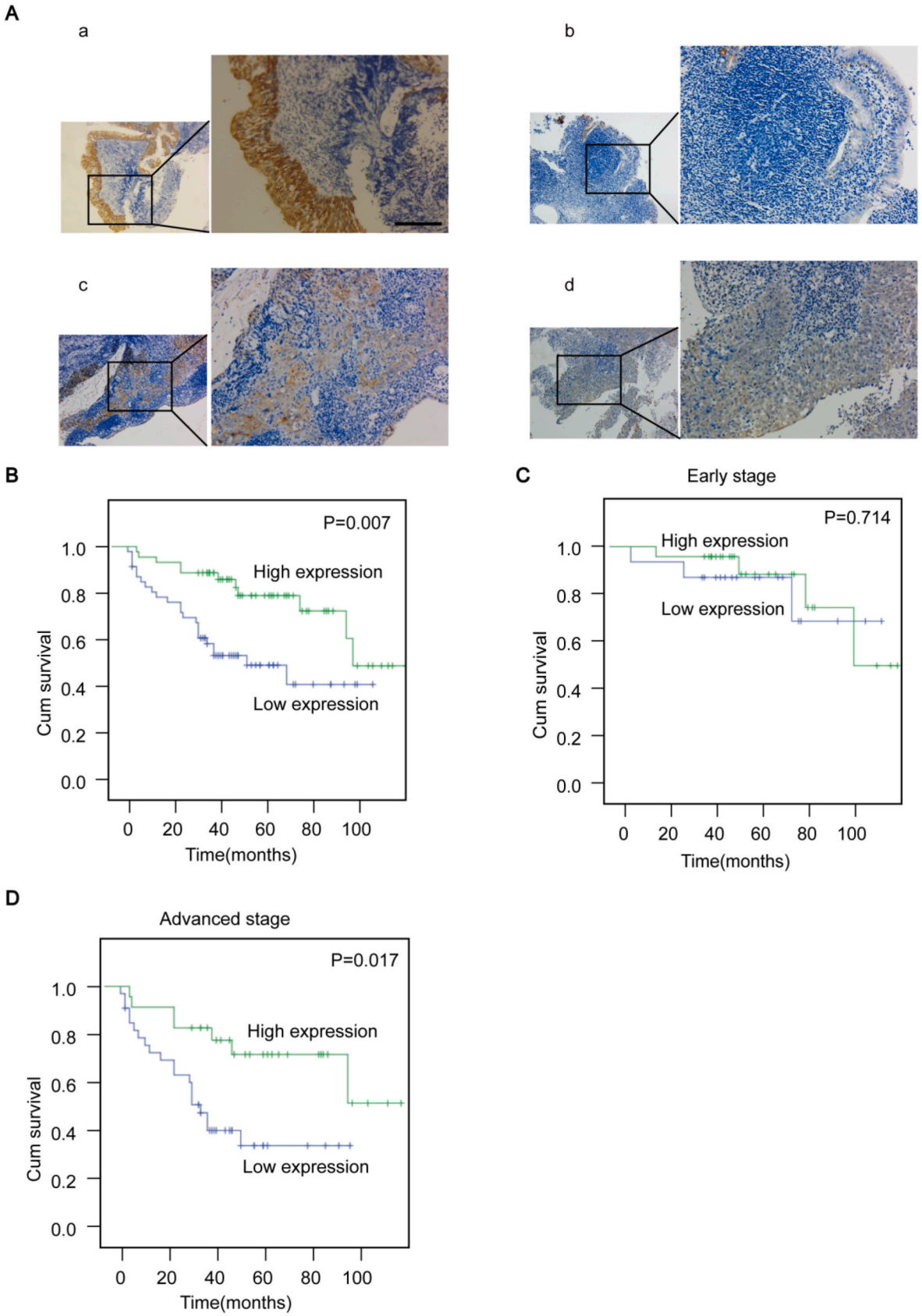

Fig. 7. Clinicopathologic characteristics of ENKUR expression in nasopharyngeal carcinoma (NPC). (A) Immunohistochemistry (IHC) staining intensities of ENKUR were assessed in tissues (a: strong expression of ENKUR in nasopharyngeal samples; b: weak expression of ENKUR in nasopharyngeal tissue; c: strong expression of ENKUR in NPC samples; d: weak expression of ENKUR in NPC tissue). (scale bar:250 μm) (B) Kaplan-Meier survival analysis with a log-rank test was conducted according to ENKUR expression. (C–D) Stratum analysis of the overall survival of patients with NPC was performed according to ENKUR expression.

Table 1
The expression of ENKUR in NPC and NP.

Group	Case	ENKUR expression		P value
		Low expression	High expression	
Cancer	121	62	59	p = 0.001
Normal epithelium	32	6	26	

NPC, nasopharyngeal carcinoma, NP normal epithelium.
*χ^2 test was applied to access ENKUR expression of NPC and NP.

Table 2
Correlation of ENKUR protein expression with clinicalpathological parameters.

parameters	Case	Low expression	High expression	Pvalue
Age(y)				
<50	69	34	35	0.619
≥50	52	28	24	
Sex				
Male	91	48	43	0.563
Female	30	14	16	
Clinical stages				
I/II	48	19	29	0.038
III/IV	73	43	30	
T stage				
T1/T2	32	11	21	0.026
T3/T4	89	51	38	
N stage				
N0/N1	59	31	28	0.780
N2/N3	62	31	31	
M stage				
M0	101	47	54	0.020
M1	20	15	5	

NPC, nasopharyngeal carcinoma.
*χ^2 test was applied to access the correlation between the clinicopathologic parameters and ENKUR expression.

Table 3
Univariate and multivariate Cox regression analysis in 121 NPC patients.

Clinical characters	Univariate analysis			Multivariate analysis		
	HR	95% CI	P value	HR	95% CI	P value
ENKUR expression						
low vs high	0.381	0.184–0.786	0.009	0.413	0.194–0.879	0.022
Sex						
male vs female	0.435	0.167–1.139	0.09			
Age						
<50 vs≥50	1.456	0.742–2.855	0.274			
Clinical stages						
I/II vs III/IV	3.022	1.315–6.945	0.009	2.557	1.062–6.156	0.036
T stage						
T1/T2 vs T3/T4	1.496	0.650–3.443	0.344			
N stage						
N0/NI vs N2/N3	2.506	1.214–5.174	0.013	1.674	0.742–3.773	0.214
M stage						
M0 vs M1	3.469	1.712–7.513	0.001	2.676	1.197–5.980	0.016

*$p < 0.05$ statistically significant.
T, tumor size; N, lymph node; M, distant metastasis; HR, hazard ratio; 95%CI, 95% confidence interval.

MYH9 and myosin_tail interacted with ENKUR, which demonstrated the significance of these two functional domains in NPC pathogenesis. We also found that ENKUR suppressed the mRNA and protein levels of MYH9 in NPC. MYH9 activated Wnt/β-catenin and the transcription factor c-Jun is a downstream driver of the pathway. Furthermore, our team has found that c-Jun transcriptionally activated MYH9, thus forming the positive regulatory loop MYH9/β-catenin/c-Jun in HCC [15]. In this study, we observed that ENKUR bound to β-catenin via its enkurin domain and reduced its nuclear translocation, which thus decreased c-Jun-dependent positive transcriptional regulation of MYH9 in NPC cells. These data revealed that ENKUR decreased MYH9 expression by combining with β-catenin and repressed its accumulation in the nucleus to decrease the transcriptional regulation of c-Jun. The data from this study revealed that ENKUR not only interacts with MYH9 but also reduces the MYH9 level via suppression of β-catenin/c-Jun-dependent transcription.

p53 is a classical tumor suppressor gene in a many types of tumors [38]. Prior studies have clarified that the mutation rate of p53 is quite low in NPC [39,40], and p53 inhibits EMT in many tumors [41–44]. In this study, ENKUR overexpression increased the protein level of p53 and MYH9 restored p53 expression, but not at the mRNA level. Furthermore, ENKUR improved the stability of the p53 protein but MYH9 overexpression reversed the stability change of p53. We speculated that the ENKUR/MYH9 signal modulates the expression of the p53 protein via the ubiquitin proteasome pathway. Previous research had shown that the E3 ubiquitin ligase UBE3A combined with p53 to decrease its protein level, which promoted Snail-mediated EMT in tumors [16–18]. Then GeneMANIA database was used to predict the interaction between MYH9 and p53 or UBE3A and we found that MYH9 is the potential interaction protein of p53 and UBE3A. Overexpression of MYH9 increased the combination of p53 and UBE3A, which promoted UBE3A-mediated ubiquitin degradation of p53 and upregulated EMT signals. These data revealed that MYH9 recruits UBE3A to degrade p53 via its ubiquitination and finally activates EMT signals.

In a previous study, we confirmed that CB induces the mRNA and protein levels of ENKUR in NPC cells. These data suggested that CB mainly induces ENKUR at a transcriptional level. C-Jun as an oncogenic transcription factor modulates many gene levels by binding to their promoters [45,46]. Interestingly, c-Jun was predicted as a candidate transcription factor of ENKUR. Our prior studies demonstrated that c-Jun [47,48] is a downstream positive regulator of the PI3K/AKT oncogenic signal [49,50], whereas CB inhibits the PI3K/AKT/c-Jun signal in NPC. We suspected that CB induces ENKUR expression through activation of PI3K/AKT/c-Jun-meditated transcription suppression in NPC. To explore this hypothesis, we confirmed that c-Jun binds to ENKUR promoter and negatively regulates its expression. We also found that PI3K inactivation by LY294002 suppressed the PI3K/AKT/c-Jun signal, which thus induced ENKUR expression in NPC.

Finally, to determine whether ENKUR participated in CB-mediated suppression of malignant phenotypes in NPC, ENKUR was knocked down in CB-treated NPC cells. We observed that cell migration and invasion abilities were enhanced. In addition, ENKUR-modulated downstream β-catenin/c-Jun/MYH9 and EMT signals were reversed.

In clinical samples, we observed that ENKUR expression was markedly upregulated in NP tissues compared with NPC tissues. Increased ENKUR expression was negatively correlated with clinical stages, T stage, and M stage, and positively related with overall survival time for patients with NPC. In addition, ENKUR expression, clinical stages and M classifications were identified as independent prognostic factors in NPC. These data revealed that ENKUR functions as an anti-tumor gene in NPC and that reduced ENKUR expression may be an important marker to predict poor prognosis for patients with NPC.

Taken together, our study revealed that a new chemical drug formulation of CB is an effective anti-metastatic treatment and enhances ENKUR expression by downregulating the PI3K/AKT/c-Jun axis. Furthermore, ENKUR as a tumor suppressor binds to MYH9, reduces its expression by recruiting β-catenin, and prevents its nuclear accumulation to decrease c-Jun transcription, which thus reduces the enlisting of E3 ligase UBE3A and decreases degradation of p53, an important anti-tumor gene that decreases EMT via UBE3A-mediated ubiquitination degradation. Our data demonstrate that CB is a potential and effective anti-metastatic drug for NPC.

Funding

This study was supported by the National Natural Science Foundation of China(81974460,81572649,81872198), the Scientific Research Project of Guangdong Provincial Bureau of Traditional Chinese Medicine (No. 20193010), the People's Livelihood Science and Technology grant of Guangzhou Municipal Science and Technology Project (No. 201803010023), Nature Science Fund of Guangdong Province (2021A1515012430, 2020A1515010176), Nature Science Fund of Hainan Province, Discipline construction project of Guangdong Medical University(4SG21011G).

CRediT author statement

Rentao Hou: Methodology, Software, Analysis and interpretation of data, Investigation, Drafting of the manuscript, Statistical analysis, Xiong Liu: Resources, Funding acquisition, Project administration, Drafting of the manuscript, technical and material support, Huiling Yang: Methodology, Drafting of the manuscript, Visualization, Funding acquisition, Shuting Deng: Software, Analysis and interpretation of data, Statistical analysis, Chao Cheng: Resources, Funding acquisition, Drafting of the manuscript, Project administration, Jiahao Liu: Validation, Investigation, Yonghao Li: Analysis and interpretation of data, Investigation, Yewei Zhang: Investigation, Jingwen Jiang: Methodology, Zhibo Zhu: English edition, Yun Su: Statistical analysis, Liyang Wu: Investigation, Yingying Xie: Software, Xiaoning Li: Analysis and interpretation of data, Wenmin Li: Methodology, Zhen Liu: Critical revision of the manuscript for important intellectual content, technical and material support, Weiyi Fang: Supervision, Funding acquisition.

Declaration of competing interest

Prof. Fang has a pending patent on cinobufagin (No. 201910399834.7). All authors declare that no support, financial or otherwise, has been received from any organization that may have an interest in the submitted work.

Acknowledgement

Not applicable.

Appendix A. Supplementary data

Supplementary data related to this article can be found at https://doi.org/10.1016/j.canlet.2022.01.025.

Abbreviations

NPC	nasopharyngeal carcinoma
CB	cinobufagin
DDP	cisplatin
DMSO	dimethyl sulfoxide
ChIP	chromatin immunoprecipitation
Co-IP	co-Immunoprecipitation
CHX	cycloheximid
EMSA	electrophoretic mobility shift assay
EMT	epithelial–mesenchymal transition

References

[1] R. Nguyen, S. Da Won Bae, L. Qiao, J. George, Developing liver organoids from induced pluripotent stem cells (iPSCs): an alternative source of organoid generation for liver cancer research, Cancer Lett. 508 (2021) 13–17.
[2] R. Piranlioglu, E. Lee, M. Ouzounova, R.J. Bollag, A.H. Vinyard, A.S. Arbab, et al., Primary tumor-induced immunity eradicates disseminated tumor cells in syngeneic mouse model, Nat. Commun. 10 (2019).
[3] X. Wang, C. Wang, J. Guan, B. Chen, L. Xu, C. Chen, Progress of breast cancer basic research in China, Int. J. Biol. Sci. 17 (2021) 2069–2079.
[4] Q. Wu, L. Jiang, S.C. Li, Q.J. He, B. Yang, J. Cao, Small molecule inhibitors targeting the PD-1/PD-L1 signaling pathway, Acta Pharmacol. Sin. 42 (2021) 1–9.
[5] S. Valastyan, R.A. Weinberg, Tumor metastasis: molecular insights and evolving paradigms, Cell 147 (2011) 275–292.
[6] G. Dai, D. Zheng, W. Guo, J. Yang, A. Cheng, Cinobufagin induces apoptosis in osteosarcoma cells via the mitochondria-mediated apoptotic pathway, Cell. Physiol. Biochem. 46 (2018) 1134–1147.
[7] Y. Bai, X. Wang, M. Cai, C. Ma, Y. Xiang, W. Hu, et al., Cinobufagin suppresses colorectal cancer growth via STAT3 pathway inhibition, Am J Cancer Res 11 (2021) 200–214.
[8] E. Apryani, U. Ali, Z. Wang, H. Wu, X. Mao, K.A. Ahmad, et al., The spinal microglial IL-10/β-endorphin pathway accounts for cinobufagin-induced mechanical antiallodynia in bone cancer pain following activation of α7-nicotinic acetylcholine receptors, J. Neuroinflammation 17 (2020).
[9] Z. Xu, F. Wang, M. Gao, X. Chen, N. Shan, S. Cheng, et al., Cardiotonic steroids attenuate ERK phosphorylation and generate cell cycle arrest to block human hepatoma cell growth, J. Steroid Biochem. Mol. Biol. 125 (2011) 181–191.
[10] Z. Pan, X. Zhang, P. Yu, X. Chen, P. Lu, M. Li, et al., Cinobufagin induces cell cycle arrest at the G2/M phase and promotes apoptosis in malignant melanoma cells, Front. Oncol. 9 (2019) 853.
[11] Z. Pan, Y. Luo, Y. Xia, X. Zhang, Y. Qin, W. Liu, et al., Cinobufagin induces cell cycle arrest at the S phase and promotes apoptosis in nasopharyngeal carcinoma cells, Biomed. Pharmacother. 122 (2020) 109763.
[12] G.H. Kim, X.Q. Fang, W.J. Lim, J. Park, T.B. Kang, J.H. Kim, et al., Cinobufagin suppresses melanoma cell growth by inhibiting LEF1, Int. J. Mol. Sci. 21 (2020).
[13] Y. Li, X. Liu, X. Lin, M. Zhao, Y. Xiao, C. Liu, et al., Chemical compound cinobufotalin potently induces FOXO1-stimulated cisplatin sensitivity by antagonizing its binding partner MYH9, Signal Transduct. Targeted Ther. 4 (2019), 48-12.
[14] Y. Liu, Q. Jiang, X. Liu, X. Lin, Z. Tang, C. Liu, et al., Cinobufotalin powerfully reversed EBV-miR-BART22-induced cisplatin resistance via stimulating MAP2K4 to antagonize non-muscle myosin heavy chain IIA/glycogen synthase 3β/β-catenin signaling pathway, EBioMedicine 48 (2019) 386–404.
[15] X. Lin, A.M. Li, Y.H. Li, R.C. Luo, Y.J. Zou, Y.Y. Liu, et al., Silencing MYH9 blocks HBx-induced GSK3beta ubiquitination and degradation to inhibit tumor stemness in hepatocellular carcinoma, Signal Transduct. Targeted Ther. 5 (2020) 13.
[16] Y.H. Jiang, D. Armstrong, U. Albrecht, C.M. Atkins, J.L. Noebels, G. Eichele, et al., Mutation of the Angelman ubiquitin ligase in mice causes increased cytoplasmic p53 and deficits of contextual learning and long-term potentiation, Neuron 21 (1998) 799–811.
[17] S. Kohli, A. Bhardwaj, R. Kumari, S. Das, SIRT6 is a target of regulation by UBE3A that contributes to liver tumorigenesis in an ANXA2-dependent manner, Cancer Res. 78 (2018) 645–658.
[18] C. Sailer, F. Offensperger, A. Julier, K. Kammer, R. Walker-Gray, M.G. Gold, et al., Structural dynamics of the E6AP/UBE3A-E6-p53 enzyme-substrate complex, Nat. Commun. 9 (2018).
[19] D. Li, Y. Wang, C. Li, Q. Wang, B. Sun, H. Zhang, et al., Cancer-speci fi c calcium nanoregulator suppressing the generation and circulation of circulating tumor cell clusters for enhanced anti-metastasis combinational chemotherapy, Acta Pharm. Sin. B 11 (2021) 3262–3271.
[20] Q. Zhang, F. Liu, W. Chen, H. Miao, H. Liang, Z. Liao, et al., The role of RNA m5 C modification in cancer metastasis, Int. J. Biol. Sci. 17 (2021) 3369–3380.
[21] Y. Liang, X. Deng, X. Lin, L. Jiang, X. Huang, Z. Mo, et al., RASSF1A inhibits PDGFB-driven malignant phenotypes of nasopharyngeal carcinoma cells in a YAP1-dependent manner, Cell Death Dis. 11 (2020).
[22] C.L. Luo, X.C. Xu, C.J. Liu, S. He, J.R. Chen, Y.C. Feng, et al., RBFOX2/GOLIM4 splicing Axis Activates vesicular transport pathway to promote nasopharyngeal carcinogenesis, Adv. Sci. 8 (2021) 2004852.
[23] M. Frikha, A. Auperin, Y. Tao, F. Elloumi, N. Toumi, P. Blanchard, et al., A randomized trial of induction docetaxel–cisplatin–5FU followed by concomitant cisplatin-RT versus concomitant cisplatin-RT in nasopharyngeal carcinoma (GORTEC 2006-02), Ann. Oncol. 29 (2018) 731–736.
[24] N.L. Syn, P.L. Lim, L.R. Kong, L. Wang, A.L. Wong, C.M. Lim, et al., Pan-CDK inhibition augments cisplatin lethality in nasopharyngeal carcinoma cell lines and xenograft models, Signal Transduct. Targeted Ther. 3 (2018) 9.
[25] C. Xue, Y. Huang, P.Y. Huang, Q.T. Yu, J.J. Pan, L.Z. Liu, et al., Phase II study of sorafenib in combination with cisplatin and 5-fluorouracil to treat recurrent or metastatic nasopharyngeal carcinoma, Ann. Oncol. 24 (2013) 1055–1061.
[26] S.P. Chen, Q. Yang, C.J. Wang, L.J. Zhang, Y. Fang, F.Y. Lei, et al., Transducin beta-like 1 X-linked receptor 1 suppresses cisplatin sensitivity in nasopharyngeal carcinoma via activation of NF-kappaB pathway, Mol. Cancer 13 (2014) 195.
[27] H. Peng, J. Zhang, P. Zhang, L. Chen, L. Tang, X. Yang, et al., ARNTL hypermethylation promotes tumorigenesis and inhibits cisplatin sensitivity by activating CDK5 transcription in nasopharyngeal carcinoma, J. Exp. Clin. Cancer Res. 38 (2019).
[28] Z. Cui, T. Pu, Y. Zhang, J. Wang, Y. Zhao, Long non-coding RNA LINC00346 contributes to cisplatin resistance in nasopharyngeal carcinoma by repressing miR-342-5p, Open Biol. 10 (2020) 190286.
[29] J. Li, Y. Wang, Y. Song, Z. Fu, W. Yu, miR-27a regulates cisplatin resistance and metastasis by targeting RKIP in human lung adenocarcinoma cells, Mol. Cancer 13 (2014) 193.
[30] X. Zhang, T. Liu, Y. Zhang, F. Liu, H. Li, D. Fang, et al., Elucidation of the differences in cinobufotalin's pharmacokinetics between normal and

diethylnitrosamine-injured rats: the role of P-glycoprotein, Front. Pharmacol. 10 (2019).
[31] W. Ren, S. Chen, Y. Liao, S. Li, J. Ge, F. Tao, et al., Near-infrared fluorescent carbon dots encapsulated liposomes as multifunctional nano-carrier and tracer of the anticancer agent cinobufagin in vivo and in vitro, Colloids Surf. B Biointerfaces 174 (2019) 384–392.
[32] K.A. Sutton, M.K. Jungnickel, Y. Wang, K. Cullen, S. Lambert, H.M. Florman, Enkurin is a novel calmodulin and TRPC channel binding protein in sperm, Dev. Biol. 274 (2004) 426–435.
[33] Q. Ma, Y. Lu, J. Lin, Y. Gu, ENKUR acts as a tumor suppressor in lung adenocarcinoma cells through PI3K/Akt and MAPK/ERK signaling pathways, J. Cancer 10 (2019) 3975–3984.
[34] Q. Ma, Y. Lu, Y. Gu, ENKUR is involved in the regulation of cellular biology in colorectal cancer cells via PI3K/Akt signaling pathway, Technol. Cancer Res. Treat. 18 (2019), 153303381984143.
[35] N.H. Ing, L. Berghman, D. Abi-Ghanem, K. Abbas, A. Kaushik, P.K. Riggs, et al., Marinobufagenin regulates permeability and gene expression of brain endothelial cells, Am. J. Physiol. Regul. Integr. Comp. Physiol. 306 (2014) R918–R924.
[36] I. Sillitoe, T.E. Lewis, A. Cuff, S. Das, P. Ashford, N.L. Dawson, et al., CATH: comprehensive structural and functional annotations for genome sequences, Nucleic Acids Res. 43 (2015) D376–D381.
[37] J.G. Lees, N.L. Dawson, I. Sillitoe, C.A. Orengo, Functional innovation from changes in protein domains and their combinations, Curr. Opin. Struct. Biol. 38 (2016) 44–52.
[38] J. Sheng, X. He, W. Yu, Y. Chen, Y. Long, K. Wang, et al., p53-targeted lncRNA ST7-AS1 acts as a tumour suppressor by interacting with PTBP1 to suppress the Wnt/β-catenin signalling pathway in glioma, Cancer Lett. 503 (2021) 54–68.
[39] L. Li, L. Guo, Y. Tao, S. Zhou, Z. Wang, W. Luo, et al., Latent membrane protein 1 of Epstein-Barr virus regulates p53 phosphorylation through MAP kinases, Cancer Lett. 255 (2007) 219–231.
[40] Y. Sun, G. Hegamyer, Y.J. Cheng, A. Hildesheim, J.Y. Chen, I.H. Chen, et al., An infrequent point mutation of the p53 gene in human nasopharyngeal carcinoma, Proc. Natl. Acad. Sci. U. S. A. 89 (1992) 6516–6520.
[41] H.M. Li, Y.R. Bi, Y. Li, R. Fu, W.C. Lv, N. Jiang, et al., A potent CBP/p300-Snail interaction inhibitor suppresses tumor growth and metastasis in wild-type p53-expressing cancer, Sci. Adv. 6 (2020), eaaw8500.
[42] Y. Wang, F. Bu, C. Royer, S. Serres, J.R. Larkin, M.S. Soto, et al., ASPP2 controls epithelial plasticity and inhibits metastasis through β-catenin-dependent regulation of ZEB1, Nat. Cell Biol. 16 (2014) 1092–1104.
[43] A. Puisieux, T. Brabletz, J. Caramel, Oncogenic roles of EMT-inducing transcription factors, Nat. Cell Biol. 16 (2014) 488–494.
[44] T.M. Jao, W.H. Fang, S.C. Ciou, S.L. Yu, Y.L. Hung, W.T. Weng, et al., PCDH10 exerts tumor-suppressor functions through modulation of EGFR/AKT axis in colorectal cancer, Cancer Lett. 499 (2021) 290–300.
[45] L. Liu, Y. Ning, J. Yi, J. Yuan, W. Fang, Z. Lin, et al., miR-6089/MYH9/beta-catenin/c-Jun negative feedback loop inhibits ovarian cancer carcinogenesis and progression, Biomed. Pharmacother. 125 (2020) 109865.
[46] C. Liu, X. Peng, Y. Li, S. Liu, R. Hou, Y. Zhang, et al., Positive feedback loop of FAM83A/PI3K/AKT/c-Jun induces migration, invasion and metastasis in hepatocellular carcinoma, Biomed. Pharmacother. 123 (2020) 109780.
[47] M. Zhao, R. Luo, Y. Liu, L. Gao, Z. Fu, Q. Fu, et al., miR-3188 regulates nasopharyngeal carcinoma proliferation and chemosensitivity through a FOXO1-modulated positive feedback loop with mTOR-p-PI3K/AKT-c-JUN, Nat. Commun. 7 (2016) 11309.
[48] Z. Liu, J. Liu, Y. Li, H. Wang, Z. Liang, X. Deng, et al., VPS33B suppresses lung adenocarcinoma metastasis and chemoresistance to cisplatin, Genes Dis. 8 (2021) 307–319.
[49] Y.Y. Zhao, J. Jia, J.J. Zhang, Y.P. Xun, S.J. Xie, J.F. Liang, et al., Inhibition of histamine receptor H3 suppresses the growth and metastasis of human non-small cell lung cancer cells via inhibiting PI3K/Akt/mTOR and MEK/ERK signaling pathways and blocking EMT, Acta Pharmacol. Sin. 42 (2021) 1288–1297.
[50] L. Wang, Z. Zhang, X. Yu, Q. Li, Q. Wang, A. Chang, et al., SOX9/miR-203a axis drives PI3K/AKT signaling to promote esophageal cancer progression, Cancer Lett. 468 (2020) 14–26.